
Dense Transformer Networks

Jun Li

School of Electrical Engineering
and Computer Science
Washington State University
Pullman, WA 99163
jun.li3@wsu.edu

Yongjun Chen

School of Electrical Engineering
and Computer Science
Washington State University
Pullman, WA 99163
yongjun.chen@wsu.edu

Lei Cai

School of Electrical Engineering
and Computer Science
Washington State University
Pullman, WA 99163
lei.cai@wsu.edu

Ian Davidson

Computer Science Department
University of California, Davis
Davis, CA 95616
davidson@cs.ucdavis.edu

Shuiwang Ji

School of Electrical Engineering
and Computer Science
Washington State University
Pullman, WA 99163
sjieecs.wsu.edu

Abstract

The key idea of current deep learning methods for dense prediction is to apply a model on a regular patch centered on each pixel to make pixel-wise predictions. These methods are limited in the sense that the patches are determined by network architecture instead of learned from data. In this work, we propose the dense transformer networks, which can learn the shapes and sizes of patches from data. The dense transformer networks employ an encoder-decoder architecture, and a pair of dense transformer modules are inserted into each of the encoder and decoder paths. The novelty of this work is that we provide technical solutions for learning the shapes and sizes of patches from data and efficiently restoring the spatial correspondence required for dense prediction. The proposed dense transformer modules are differentiable, thus the entire network can be trained. We apply the proposed networks on natural and biological image segmentation tasks and show superior performance is achieved in comparison to baseline methods.

1 Introduction

In recent years, deep convolution neural networks (CNNs) have achieved promising performance on many artificial intelligence tasks, including image recognition [21, 19], object detection [29, 13], and segmentation [12, 26, 27, 3, 31]. Among these tasks, dense prediction tasks take images as inputs and generate output maps with similar or the same size as the inputs. For example, in image semantic segmentation, we need to predict a label for each pixel on the input images [23, 25]. Other examples include depth estimation [20, 10], image super-resolution [8], and surface normal prediction [9]. These tasks can be generally considered as image-to-image translation problems in which inputs are images, and outputs are label maps [16].

Given the success of deep learning methods on image-related applications, numerous recent attempts have been made to solve dense prediction problems using CNNs. A central idea of these methods is to extract a square patch centered on each pixel and apply CNNs on each of them to compute the label of the center pixel. The efficiency of these approaches can be improved by using fully convolutional or encoder-decoder networks. Specifically, fully convolutional networks [23] replace fully connected layers with convolutional layers, thereby allowing inputs of arbitrary size during both training and test. In contrast, deconvolution networks [25] employ an encoder-decoder architecture. The encoder path extracts high-level representations using convolutional and pooling layers. The decoder path uses deconvolutional and up-pooling layers to recovering the original spatial resolution. In order to transmit information directly from encoder to decoder, the U-Net [28] adds skip connections [14] between the corresponding encoder and decoder layers. A common property of all these methods is that the label of any pixel is determined by a regular (usually square) patch centered on that pixel. Although these methods have achieved considerable practical success, there are limitations inherent in them. For example, once the network architecture is determined, the patches used to predict the label of each pixel is completely determined, and they are commonly of the same size for all pixels. In addition, the patches are usually of a regular shape, e.g., squares.

In this work, we propose the dense transformer networks to address these limitations. Our method follows the encoder-decoder architecture in which the encoder converts input images into high-level representations, and the decoder tries to make pixel-wise predictions by recovering the original spatial resolution. Under this framework, the label of each pixel is also determined by a local patch on the input. Our method allows the size and shape of every patch to be adaptive and data-dependent. In order to achieve this goal, we propose to insert a spatial transformer layer [17] in the encoder part of our network. We propose to use nonlinear transformations, such as these based on thin-plate splines [30, 2]. The nonlinear spatial transformer layer transforms the feature maps into a different space. Therefore, performing regular convolution and pooling operations in this space corresponds to performing these operations on irregular patches of different sizes in the original space. Since the nonlinear spatial transformations are learned automatically from data, this corresponds to learning the size and shape of each patch to be used as inputs for convolution and pooling operations.

There has been prior work on allowing spatial transformations or deformations in deep networks [17, 6], but they do not address the spatial correspondence problem, which is critical in dense prediction tasks. The difficulty in applying spatial transformations to dense prediction tasks lies in that the spatial correspondence between input images and output label maps needs to be preserved. A key innovation of this work is that we provide a new technical solution that not only allows data-dependent learning of patches but also enables the preservation of spatial correspondence. Specifically, although the patches used to predict pixel labels could be of different sizes and shapes, we expect the patches to be in the spatial vicinity of pixels whose labels are to be predicted. By applying the nonlinear spatial transformer layers in the encoder path as described above, the spatial locations of units on the intermediate feature maps after the spatial transformation layer may not be preserved. Thus a reverse transformation is required to restore the spatial correspondence.

In order to restore the spatial correspondence between inputs and outputs, we propose to add a corresponding decoder layer. A technical challenge in developing the decoder layer is that we need to map values of units arranged on input regular grid to another set of units arranged on output grid, while the nonlinear transformation could map input units to arbitrary locations on the output map. We develop an interpolation method to address this challenge. Altogether, our work results in the dense transformer networks, which allow the prediction of each pixel to adaptively choose the input patch in a data-dependent manner. The dense transformer networks can be trained end-to-end, and gradients can be back-propagated through both the encoder and decoder layers. Experimental results on natural and biological images demonstrate the effectiveness of the proposed dense transformer networks.

2 Spatial Transformer Networks Based on Thin-Plate Spline

Spatial transformer networks [17] are deep models containing spatial transformer layers. These layers explicitly compute a spatial transformation of the input feature maps. They can be inserted into convolutional neural networks to perform explicit spatial transformations. The spatial transformer layers consist of three components; namely, the localization network, grid generator and sampler.

The localization network takes a set of feature maps as input and generates parameters to control the transformation. If there are multiple feature maps, the same transformation is applied to all of them. The grid generator constructs transformation mapping between input and output grids based on parameters computed from the localization network. The sampler computes output feature maps based on input feature maps and the output of grid generator. The spatial transformer layers are generic and different types of transformations, e.g., affine transformation, projective transformation, and thin-plate spline (TPS), can be used. Our proposed work is based on the TPS transformation, and it is not described in detail in the original paper [17]. Thus we provide more details below.

2.1 Localization Network

When there are multiple feature maps, the same transformation is applied to all of them. Thus, we assume there is only one input feature map below. The TPS transformation is determined by $2K$ fiducial points among which K points lie on the input feature map and the other K points lie on the output feature map. On the output feature map, the K fiducial points, whose coordinates are denoted as $\tilde{F} = [\tilde{f}_1, \tilde{f}_2, \dots, \tilde{f}_K] \in \mathbb{R}^{2 \times K}$, are evenly distributed on a fixed regular grid, where $\tilde{f}_i = [\tilde{x}_i, \tilde{y}_i]^T$ denotes the coordinates of the i th point. The localization network is used to learn the K fiducial points $F = [f_1, f_2, \dots, f_K] \in \mathbb{R}^{2 \times K}$ on the input feature map. Specifically, the localization network, denoted as $f_{loc}(\cdot)$, takes the input feature maps $U \in \mathbb{R}^{H \times W \times C}$ as input, where H , W and C are the height, width and number of channels of input feature maps, and generates the normalized coordinates F as the output as $F = f_{loc}(U)$.

A cascade of convolutional, pooling and fully-connected layers is used to implement $f_{loc}(\cdot)$. The output of the final fully-connected layer is the coordinates F on the input feature map. Therefore, the number of output units of the localization network is $2K$. In order to ensure that the outputs are normalized between -1 and 1 , the activation function $\tanh(\cdot)$ is used in the fully-connected layer. Since the localization network is differentiable, the K fiducial points can be learned from data using error back-propagation.

2.2 Grid Generator

For each unit lying on a regular grid on the output feature map, the grid generator computes the coordinate of the corresponding unit on the input feature map. This correspondence is determined by the coordinates of the fiducial points F and \tilde{F} . Given the evenly distributed K points $\tilde{F} = [\tilde{f}_1, \tilde{f}_2, \dots, \tilde{f}_K]$ on the output feature map and the K fiducial points $F = [f_1, f_2, \dots, f_K]$ generated by the localization network, the transformation matrix T in TPS can be expressed as follows:

$$T = \left(\Delta_{\tilde{F}}^{-1} \times \begin{bmatrix} F^T \\ \mathbf{0}_{3 \times 2} \end{bmatrix} \right)^T \in \mathbb{R}^{2 \times (K+3)}, \quad (1)$$

where $\Delta_{\tilde{F}} \in \mathbb{R}^{(K+3) \times (K+3)}$ is a matrix determined only by \tilde{F} as

$$\Delta_{\tilde{F}} = \begin{bmatrix} \mathbf{1}^{K \times 1} & \tilde{F}^T & R \\ \mathbf{0}^{1 \times 1} & \mathbf{0}^{1 \times 2} & \mathbf{1}^{1 \times K} \\ \mathbf{0}^{2 \times 1} & \mathbf{0}^{2 \times 2} & \tilde{F} \end{bmatrix} \in \mathbb{R}^{(K+3) \times (K+3)}, \quad (2)$$

where $R \in \mathbb{R}^{K \times K}$, and its elements are defined as $r_{i,j} = d_{i,j}^2 \ln d_{i,j}^2$, and $d_{i,j}$ denotes the Euclidean distance between \tilde{f}_i and \tilde{f}_j .

Through the mapping, each unit $(\tilde{x}_i, \tilde{y}_i)$ on the output feature map corresponds to unit (x_i, y_i) on the input feature map. To achieve this mapping, we represent the units on the regular output grid by $\{\tilde{p}_i\}_{i=1}^{\tilde{H} \times \tilde{W}}$, where $\tilde{p}_i = [\tilde{x}_i, \tilde{y}_i]^T$ is the (x, y) -coordinates of the i th unit on output grid, and \tilde{H} and \tilde{W} are the height and width of output feature maps. Note that the fiducial points $\{\tilde{f}_i\}_{i=1}^K$ are a subset of the points $\{\tilde{p}_i\}_{i=1}^{\tilde{H} \times \tilde{W}}$, which are the set of all points on the regular output grid.

To apply the transformation, each point \tilde{p}_i is first extended from \mathbb{R}^2 space to \mathbb{R}^{K+3} space as $\tilde{q}_i = [1, \tilde{x}_i, \tilde{y}_i, s_{i,1}, s_{i,2}, \dots, s_{i,K}]^T \in \mathbb{R}^{K+3}$, where $s_{i,j} = e_{i,j}^2 \ln e_{i,j}^2$, and $e_{i,j}$ is the Euclidean distance between \tilde{p}_i and \tilde{f}_j . Then the transformation can be expressed as

$$p_i = T\tilde{q}_i, \quad (3)$$

where T is defined in Eq. (1). By this transformation, each coordinate $(\tilde{x}_i, \tilde{y}_i)$ on the output feature map corresponds to a coordinate (x_i, y_i) on the input feature map. Note that the transformation T is defined so that the points \tilde{F} map to points F .

2.3 Sampler

The sampler generates output feature maps based on input feature maps and the outputs of grid generator. Each unit \tilde{p}_i on the output feature map corresponds to a unit p_i on the input feature map as computed by Eq. (3). However, the coordinates $p_i = (x_i, y_i)^T$ computed by Eq. (3) may not lie exactly on the input regular grid. In these cases, the output values need to be interpolated from input values lying on regular grid. For example, a bilinear sampling method can be used to achieve this. Specifically, given an input feature map $U \in \mathbb{R}^{H \times W}$, the output feature map $V \in \mathbb{R}^{\tilde{H} \times \tilde{W}}$ can be obtained as

$$V_i = \sum_{n=1}^{\tilde{H}} \sum_{m=1}^{\tilde{W}} U_{nm} \max(0, 1 - |x_i - m|) \max(0, 1 - |y_i - n|) \quad (4)$$

for $i = 1, 2, \dots, \tilde{H} \times \tilde{W}$, where V_i is the value of pixel i , U_{nm} is the value at (n, m) on the input feature map, $p_i = (x_i, y_i)^T$, and p_i is computed from Eq. (3). By using the transformations, the spatial transformer networks have been shown to be invariant to some transformations on the inputs. Other recent studies have also attempted to make CNNs to be invariant to various transformations [18, 15, 5, 7].

3 Dense Transformer Networks

The central idea of CNN-based method for dense prediction is to extract a regular patch centered on each pixel and apply CNNs to compute the label of that pixel. A common property of these methods is that the label of each pixel is determined by a regular (typically square) patch centered on that pixel. Although these methods have been shown to be effective on dense prediction problems, they lack the ability to learn the sizes and shapes of patches in a data-dependent manner. For a given network, the size of patches used to predict the labels of each center pixel is determined by the network architecture. Although multi-scale networks have been proposed to allow patches of different sizes to be combined [12], the patch sizes are again determined by network architectures. In addition, the shapes of patches used in CNNs are invariably regular, such as squares. Ideally, the shapes of patches may depend on local image statistics around that pixel and thus should be learned from data. In this work, we propose the dense transformer networks to enable the learning of patch size and shape for each pixel.

3.1 An Encoder-Decoder Architecture

In order to address the above limitations, we propose to develop a dense transformer network model. Our model employs an encoder-decoder architecture in which the encoder path extracts high-level representations using convolutional and pooling layers and the decoder path uses deconvolution and un-pooling to recover the original spatial resolution [25, 28, 1, 24]. To enable the learning of size and shape of each patch automatically from data, we propose to insert a spatial transformer module in the encoder path in our network. As has been discussed above, the spatial transformer module transforms the feature maps into a different space using nonlinear transformations. Applying convolution and pooling operations on regular patches in the transformed space is equivalent to operating on irregular patches of different sizes in the original space. Since the spatial transformer module is differentiable, its parameters can be learned with error back-propagation algorithms. This is equivalent to learning the size and shape of each patch from data.

Although the patches used to predict pixel labels could be of different sizes and shapes, we expect the patches to include the pixel in question at least. That is, the patches should be in the spatial vicinity of pixels whose labels are to be predicted. By using the nonlinear spatial transformer layer in encoder path, the spatial locations of units on the intermediate feature maps could have been changed. That is, due to this nonlinear spatial transformation, the spatial correspondence between input images and output label maps is not retained in the feature maps after the spatial transformer layer. In order to restore this spatial correspondence, we propose to add a corresponding decoder layer, known as the

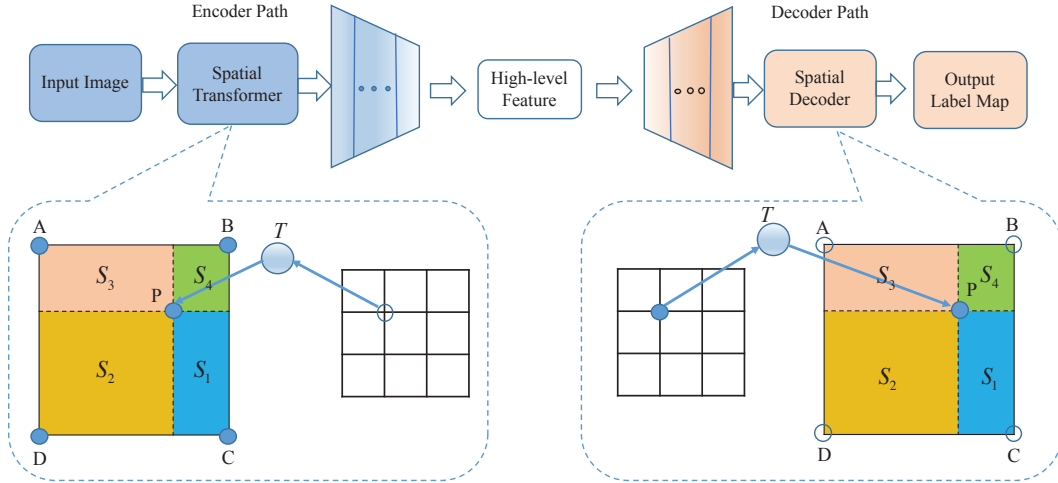


Figure 1: The proposed dense transformer networks. A pair of dense transformer modules are inserted into each of the encoder and decoder paths. In the spatial transformer module, values at points A , B , C , and D are given from the previous layer, and we need to estimate value for point P . In contrast, in the decoder layer, value at point P is given from the previous layer, and we need to estimate values for points A , B , C , and D .

dense transformer decoder layer. This decoder layer transforms the intermediate feature maps back to the original input space, thereby re-establishing the input-output spatial correspondence.

The spatial transformer module can be inserted after any layer in the encoder path while the dense transform decoder module should be inserted into the corresponding location in decoder path. In our framework, the spatial transformer module is required to not only output the transformed feature maps, but also the transformation itself that captures the spatial correspondence between input and output feature maps. This information will be used to restore the spatial correspondence in the decoder module. Note that in the spatial transformer encoder module, the transformation is computed in the backward direction, i.e., from output to input feature maps (Figure 1). In contrast, the dense transformer decoder module uses a forward direction instead; that is, a mapping from input to output feature maps. This encoder-decoder pair can be implemented efficiently by sharing the transformation parameters in these two modules.

A technical challenge in developing the dense transformer decoder layer is that we need to map values of units arranged on input regular grid to another set of units arranged on regular output grid, while the decoder could map to units at arbitrary locations on the output map. That is, while we need to compute the values of units lying on regular output grid from values of units lying on regular input grid, the mapping itself could map an input unit to an arbitrary location on the output feature map, i.e., not necessarily to a unit lying exactly on the output grid. To address this challenge, we develop a sampler method for performing interpolation. We show that the proposed samplers are differentiable, thus gradients can be propagated through these modules. This makes the entire dense transformer networks fully trainable. Formally, assume that the encoder and decoder layers are inserted after the i -th and j -th layers, respectively, then we have the following relationships:

$$U^{i+1}(p) = \text{Sampling}\{U^i(Tp)\}, \quad U^{j+1}(Tp) = U^j(p), \quad U^{j+1}(p) = \text{Sampling}\{U^{j+1}(Tp)\}, \quad (5)$$

where U^i is the feature map of the i -th layer, p is the coordinate of a point, T is the transformation defined in Eq. (1), which maps from the coordinates of the $(i+1)$ -th layer to the i -th layer, $\text{Sampling}(\cdot)$ denotes the sampler function.

From a geometric perspective, a value associated with an estimated point in bilinear interpolation in Eq. (4) can be interpreted as a linear combination of values at four neighboring grid points. The weights for linear combination are areas of rectangles determined by the estimated points and four neighboring grid points. For example, in Figure 1, when a point is mapped to P on input grid, the contributions of points A , B , C , and D to the estimated point P is determined by the areas of

the rectangles $S_1, S_2, S_3,$ and S_4 . However, the interpolation problem needs to be solved in the dense transformer decoder layer is different with the one in the spatial transformer encoder layer, as illustrated in Figure 1. Specifically, in the encoder layer, the points $A, B, C,$ and D are associated with values computed from the previous layer, and the interpolation problem needs to compute a value for P to be propagated to the next layer. In contrast, in the decoder layer, the point P is associated with a value computed from the previous layer, and the interpolation problem needs to compute values for $A, B, C,$ and D . Due to the different natures of the interpolation problems need to be solved in the encoder and decoder modules, we propose a new sampler that can efficiently interpolate over decimal points in the following section.

3.2 Decoder Sampler

In the decoder sampler, we need to estimate values of regular grid points based on those from arbitrary decimal points, i.e., those that do not lie on the regular grid. For example, in Figure 1, the value at point P is given from the previous layer. After the TPS transformation in Eq. (3), it may be mapped to an arbitrary point. Therefore, the values of grid points $A, B, C,$ and D need to be computed based on values from a set of arbitrary points. If we compute the values from surrounding points as in the encoder layer, we might have to deal with a complex interpolation problem over irregular quadrilaterals. Those complex interpolation methods may yield more accurate results, but we prefer a simpler and more efficient method in this work. Specifically, we propose a new sampling method, which distributes the value of P to the points $A, B, C,$ and D in an intuitive manner. Geometrically, the weights associated with points $A, B, C,$ and D are the area of the rectangles $S_1, S_2, S_3,$ and S_4 , respectively (Figure 1). In particular, given an input feature map $V \in \mathbb{R}^{\tilde{H} \times \tilde{W}}$, the output feature map $U \in \mathbb{R}^{H \times W}$ can be obtained as

$$S_{nm} = \sum_{i=1}^{\tilde{H} \times \tilde{W}} \max(0, 1 - |x_i - m|) \max(0, 1 - |y_i - n|), \quad (6)$$

$$U_{nm} = \frac{1}{S_{nm}} \sum_{i=1}^{\tilde{H} \times \tilde{W}} V_i \max(0, 1 - |x_i - m|) \max(0, 1 - |y_i - n|), \quad (7)$$

where V_i is the value of pixel i , $p_i = (x_i, y_i)^T$ is transformed by the shared transformation T in Eq. (1), U_{nm} is the value at the (n, m) -th location on the output feature map, S_{nm} is a normalization term that is used to eliminate the effect that different grid points may receive values from different numbers of arbitrary points, and $n = 1, 2, \dots, N, m = 1, 2, \dots, M$.

In order to allow the backpropagation of errors, we define the gradient with respect to U_{nm} as dU_{nm} . Then the gradient with respect to V_{nm} and x_i can be derived as follows:

$$dV_i = \sum_{n=1}^H \sum_{m=1}^W \frac{1}{S_{nm}} dU_{nm} \max(0, 1 - |x_i - m|) \max(0, 1 - |y_i - n|), \quad (8)$$

$$dS_{nm} = \frac{-dU_{nm}}{S_{nm}^2} \sum_{i=1}^{\tilde{H} \times \tilde{W}} V_i \max(0, 1 - |x_i - m|) \max(0, 1 - |y_i - n|), \quad (9)$$

$$dx_i = \sum_{n=1}^H \sum_{m=1}^W \left\{ \frac{dU_{nm}}{S_{nm}} V_i + dS_{nm} \right\} \max(0, 1 - |y_i - n|) \times \begin{cases} 0 & \text{if } |m - x_i| \geq 1 \\ 1 & \text{if } m \geq x_i \\ -1 & \text{if } m \leq x_i \end{cases}. \quad (10)$$

A similar gradient can be derived for dy_i . This provides us with a differentiable sampling mechanism, which enables the gradients flow back to both the input feature map and the sampling layers.

4 Experimental Evaluation

We evaluate the proposed methods on two image segmentation tasks. The U-Net [28] is adopted as our base model in both tasks, as it has achieved state-of-the-art performance on image segmentation tasks. Specifically, U-Net adds residual connections between the encoder path and decoder path to incorporate both low-level and high-level features. Other methods like SegNet [1], deconvolutional networks [32] and FCN [23] mainly differ from U-Net in the up-sampling method and do not use

Table 1: Comparison of segmentation performance between the U-Net and the proposed DTN on the PASCAL 2012 segmentation data set. Three different performance measures are used here. An arrow is attached to each measure so that \uparrow denotes higher values indicate better performance, and \downarrow denotes lower values indicate better performance.

DATA SET	MODEL	LOSS \downarrow	ACCURACY \uparrow	MEAN-IOU \uparrow
PASCAL	U-NET	0.9396	0.8117	0.4145
	DTN	0.7909	0.8367	0.5297

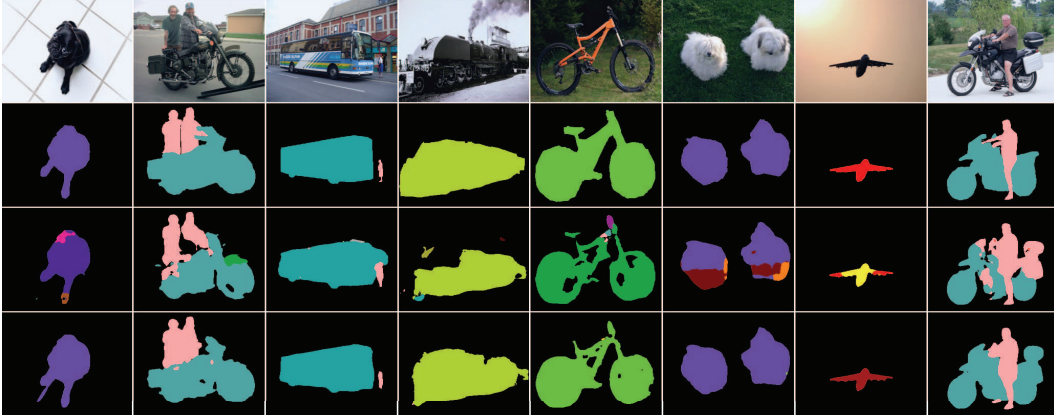


Figure 2: Sample segmentation results on the PASCAL 2012 segmentation data set. The first and second rows are the original images and the corresponding ground truth, respectively. The third and fourth rows are the segmentation results of U-Net and DTN, respectively.

residual connections. Experiments in prior work show that residual connections are important while different up-sampling methods lead to similar results. The network consists of 5 layers in the encoder path and another corresponding 5 layers in the decoder path. We use 3×3 kernels and one pixel padding to retain the size of feature maps at each level.

In order to efficiently implement the transformations, we insert the spatial encoder layer and dense transformer decoder layer into corresponding positions at the same level. Specifically, the layers are applied to the 4th layer, and their performance is compared to the basic U-Net model without spatial transformations. As for the transformation layers, we use 16 fiducial points that are evenly distributed on the output feature maps. In the dense transformer decoder layer, if there are pixels that are not selected on the output feature map, we apply an interpolation strategy over its neighboring pixels on previous feature maps to produce smooth results.

4.1 Natural Image Semantic Segmentation

We use the PASCAL 2012 segmentation data set [11] to evaluate the proposed methods on natural image semantic segmentation task. In this task, we predict one label out of a total of 21 classes for each pixel. To avoid the inconvenience of different sizes of images, we resize all the images to 256×256 . Multiple performance metrics, including loss, accuracy, and mean-IOU, are used to measure the segmentation performance, and the results are reported in Table 1. We can observe that the proposed DTN model achieves higher performance than the baseline U-Net model. Especially, it improves the mean-IOU from 0.4145 to 0.5297. Some example results along with the raw images and ground truth label maps are given in Figure 2. These results demonstrate that the proposed DTN model can boost the segmentation performance dramatically.

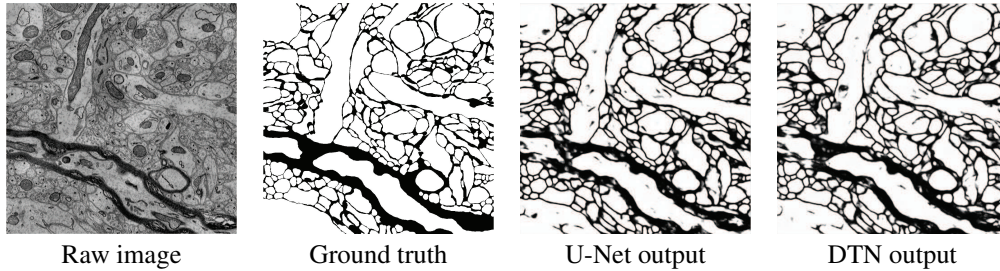


Figure 4: Example results generated by the U-Net and the proposed DTN models for the SNEMI3D data set.

4.2 Brain Electron Microscopy Image Segmentation

We evaluate the proposed methods on brain electron microscopy (EM) image segmentation task [22, 4], in which the ultimate goal is to reconstruct neurons at the micro-scale level. A critical step in neuron reconstruction is to segment the EM images. We use data set from the 3D Segmentation of Neurites in EM Images (SNEMI3D, <http://brainiac2.mit.edu/SNEMI3D/>). The SNEMI3D data set consists of 100 1024×1024 EM image slices. Since we perform 2D transformations in this work, each image slice is segmented separately in our experiments. The task is to predict each pixel as either a boundary (denoted as 1) or a non-boundary pixel (denoted as 0).

Our model can process images of arbitrary size. However, training on whole images may incur excessive memory requirement. In order to accelerate training, we randomly pick 224×224 patches from the original images and use it to train the networks. The experimental results in terms of ROC curves are provided in Figure 3. We can observe that the proposed DTN model achieves higher performance than the baseline U-Net model, improving AUC from 0.8676 to 0.8953. These results demonstrate that the proposed DTN model improves upon the baseline U-Net model, and the use of the dense transformer encoder and decoder modules in the U-Net architecture results in improved performance. Some example results along with the raw images and ground truth label maps are given in Figure 4.

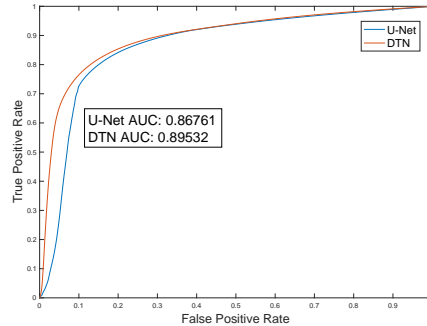


Figure 3: Comparison of the ROC curves of the U-Net and the proposed DTN model on the SNEMI3D data set.

4.3 Timing Comparison

Table 2 shows the comparison of training and prediction time between the U-Net model and the proposed DTN model on the two data sets. We can see that adding DTN layers leads to only slight increase in training and prediction time. Since the PASCAL data set is more complex than the SNEME3D data set, we use more channels when building the network of natural image segmentation task. That causes the increase of training and prediction time on the PASCAL data set as compared to SNEME3D.

5 Conclusion

In this work, we propose the dense transformer networks to enable the automatic learning of patch sizes and shapes in dense prediction tasks. This is achieved by transforming the intermediate feature maps to a different space using nonlinear transformations. A unique challenge in dense prediction tasks is that, the spatial correspondence between inputs and outputs should be preserved in order to

Table 2: Training and prediction time on the two data sets using a Tesla K40 GPU. We compare the training time of 10,000 iterations and prediction time of 2019 (PASCAL) and 40 (SNEMI3D) images for the base U-Net model and the DTN.

DATA SET	MODEL	TRAINING TIME	PREDICTION TIME
PASCAL	U-NET	378M57s	14M06s
	DTN	402M07s	15M50s
SNEMI3D	U-NET	14M18s	3M31s
	DTN	15M41s	4M02s

make pixel-wise predictions. To this end, we develop the dense transformer decoder layer to restore the spatial correspondence. The proposed dense transformer modules are differentiable. Thus the entire network can be trained from end to end. Experimental results show that adding the spatial transformer and decoder layers to existing models leads to improved performance. To the best of our knowledge, our work represents the first attempt to enable the learning of patch size and shape in dense prediction. The current study only adds one encoder layer and one decoder layer in the baseline models. We will explore the possibility of adding multiple encoder and decoder layers at different locations of the baseline model. In this work, we develop a simple and efficient decoder sampler for interpolation. A more complex method based on irregular quadrilaterals might be more accurate and will be explored in the future.

Acknowledgments

This work was supported in part by National Science Foundation grants IIS-1615035 and DBI-1641223, and by Washington State University. We gratefully acknowledge the support of NVIDIA Corporation with the donation of the Tesla K40 GPU used for this research.

References

- [1] Vijay Badrinarayanan, Alex Kendall, and Roberto Cipolla. Segnet: A deep convolutional encoder-decoder architecture for image segmentation. *arXiv preprint arXiv:1511.00561*, 2015.
- [2] Fred L. Bookstein. Principal warps: Thin-plate splines and the decomposition of deformations. *IEEE Transactions on pattern analysis and machine intelligence*, 11(6):567–585, 1989.
- [3] Liang-Chieh Chen, George Papandreou, Iasonas Kokkinos, Kevin Murphy, and Alan L. Yuille. Semantic image segmentation with deep convolutional nets and fully connected CRFs. In *Proceedings of the International Conference on Learning Representations*, 2015.
- [4] Dan Ciresan, Alessandro Giusti, Luca M Gambardella, and Jürgen Schmidhuber. Deep neural networks segment neuronal membranes in electron microscopy images. In *Advances in neural information processing systems*, pages 2843–2851, 2012.
- [5] Taco Cohen and Max Welling. Group equivariant convolutional networks. In *Proceedings of The 33rd International Conference on Machine Learning*, pages 2990–2999, 2016.
- [6] Jifeng Dai, Haozhi Qi, Yuwen Xiong, Yi Li, Guodong Zhang, Han Hu, and Yichen Wei. Deformable convolutional networks. *arXiv preprint arXiv:1703.06211*, 2017.
- [7] Sander Dieleman, Jeffrey De Fauw, and Koray Kavukcuoglu. Exploiting cyclic symmetry in convolutional neural networks. In *Proceedings of The 33rd International Conference on Machine Learning*, pages 1889–1898, 2016.
- [8] Chao Dong, Chen Change Loy, Kaiming He, and Xiaoou Tang. Image super-resolution using deep convolutional networks. *IEEE Transactions on Pattern Analysis and Machine Intelligence*, 38(2):295–307, 2016.
- [9] David Eigen and Rob Fergus. Predicting depth, surface normals and semantic labels with a common multi-scale convolutional architecture. In *Proceedings of the IEEE International Conference on Computer Vision*, pages 2650–2658, 2015.
- [10] David Eigen, Christian Puhrsch, and Rob Fergus. Depth map prediction from a single image using a multi-scale deep network. In *Advances in neural information processing systems*, pages 2366–2374, 2014.
- [11] Mark Everingham, Luc Van Gool, Christopher KI Williams, John Winn, and Andrew Zisserman. The pascal visual object classes (voc) challenge. *International journal of computer vision*, 88(2):303–338, 2010.
- [12] Clement Farabet, Camille Couprie, Laurent Najman, and Yann LeCun. Learning hierarchical features for scene labeling. *IEEE Transactions on Pattern Analysis and Machine Intelligence*, 35(8):1915–1929, 2013.
- [13] Ross Girshick, Jeff Donahue, Trevor Darrell, and Jitendra Malik. Rich feature hierarchies for accurate object detection and semantic segmentation. In *Proceedings of the IEEE conference on computer vision and pattern recognition*, pages 580–587, 2014.
- [14] Kaiming He, Xiangyu Zhang, Shaoqing Ren, and Jian Sun. Deep residual learning for image recognition. In *Proceedings of the IEEE Conference on Computer Vision and Pattern Recognition*, 2016.
- [15] João F Henriques and Andrea Vedaldi. Warped convolutions: Efficient invariance to spatial transformations. *arXiv preprint arXiv:1609.04382*, 2016.

- [16] Phillip Isola, Jun-Yan Zhu, Tinghui Zhou, and Alexei A Efros. Image-to-image translation with conditional adversarial networks. *arXiv preprint arXiv:1611.07004*, 2016.
- [17] Max Jaderberg, Karen Simonyan, Andrew Zisserman, et al. Spatial transformer networks. In *Advances in Neural Information Processing Systems*, pages 2017–2025, 2015.
- [18] Xu Jia, Bert De Brabandere, Tinne Tuytelaars, and Luc V Gool. Dynamic filter networks. In *Advances in Neural Information Processing Systems*, pages 667–675, 2016.
- [19] Alex Krizhevsky, Ilya Sutskever, and Geoffrey E Hinton. Imagenet classification with deep convolutional neural networks. In *Advances in neural information processing systems*, pages 1097–1105, 2012.
- [20] Iro Laina, Christian Rupprecht, Vasileios Belagiannis, Federico Tombari, and Nassir Navab. Deeper depth prediction with fully convolutional residual networks. In *2016 Fourth International Conference on 3D Vision*, pages 239–248. IEEE, 2016.
- [21] Y. LeCun, L. Bottou, Y. Bengio, and P. Haffner. Gradient-based learning applied to document recognition. *Proceedings of the IEEE*, 86(11):2278–2324, November 1998.
- [22] Kisuk Lee, Aleksandar Zlateski, Vishwanathan Ashwin, and H Sebastian Seung. Recursive training of 2D-3D convolutional networks for neuronal boundary prediction. In *Advances in Neural Information Processing Systems*, pages 3573–3581, 2015.
- [23] Jonathan Long, Evan Shelhamer, and Trevor Darrell. Fully convolutional networks for semantic segmentation. In *Proceedings of the IEEE Conference on Computer Vision and Pattern Recognition*, pages 3431–3440, 2015.
- [24] Alejandro Newell, Kaiyu Yang, and Jia Deng. Stacked hourglass networks for human pose estimation. In *European Conference on Computer Vision*, pages 483–499. Springer, 2016.
- [25] Hyeonwoo Noh, Seunghoon Hong, and Bohyung Han. Learning deconvolution network for semantic segmentation. In *Proceedings of the IEEE International Conference on Computer Vision*, pages 1520–1528, 2015.
- [26] Pedro Pinheiro and Ronan Collobert. Recurrent convolutional neural networks for scene labeling. In *Proceedings of the 31st International Conference on Machine Learning*, pages 82–90, 2014.
- [27] Pedro O Pinheiro, Tsung-Yi Lin, Ronan Collobert, and Piotr Dollár. Learning to refine object segments. In *European Conference on Computer Vision*, pages 75–91. Springer, 2016.
- [28] Olaf Ronneberger, Philipp Fischer, and Thomas Brox. U-net: Convolutional networks for biomedical image segmentation. In *International Conference on Medical Image Computing and Computer-Assisted Intervention*, pages 234–241. Springer, 2015.
- [29] Pierre Sermanet, David Eigen, Xiang Zhang, Michael Mathieu, Rob Fergus, and Yann LeCun. OverFeat: Integrated recognition, localization and detection using convolutional networks. In *Proceedings of the International Conference on Learning Representations*, April 2014.
- [30] Baoguang Shi, Xinggang Wang, Pengyuan Lyu, Cong Yao, and Xiang Bai. Robust scene text recognition with automatic rectification. In *Proceedings of the IEEE Conference on Computer Vision and Pattern Recognition*, pages 4168–4176, 2016.
- [31] Francesco Visin, Kyle Kastner, Aaron Courville, Yoshua Bengio, Matteo Matteucci, and Kyunghyun Cho. ReSeg: A recurrent neural network for object segmentation. *arXiv preprint arXiv:1511.07053*, 2015.
- [32] Matthew D Zeiler, Dilip Krishnan, Graham W Taylor, and Rob Fergus. Deconvolutional networks. In *Computer Vision and Pattern Recognition (CVPR), 2010 IEEE Conference on*, pages 2528–2535. IEEE, 2010.